Inference of Marine Atmospheric Boundary Layer Moisture and Temperature Structure Using Airborne Lidar and Infrared Radiometer Data

STEPHEN P. PALM

Science Systems and Applications Incorporated, Lanham, Maryland

DENISE HAGAN

Jet Propulsion Laboratory, Pasadena, California

GEARY SCHWEMMER

Laboratory for Atmospheres, NASA/Goddard Space Flight Center, Greenbelt, Maryland

S. H. MELFI

University of Maryland, Catonsville, Maryland

(Manuscript received 14 August 1996, in final form 17 June 1997)

ABSTRACT

A new technique for retrieving near-surface moisture and profiles of mixing ratio and potential temperature through the depth of the marine atmospheric boundary layer (MABL) using airborne lidar and multichannel infrared radiometer data is presented. Data gathered during an extended field campaign over the Atlantic Ocean in support of the Lidar In-space Technology Experiment are used to generate 16 moisture and temperature retrievals that are then compared with dropsonde measurements. The technique utilizes lidar-derived statistics on the height of cumulus clouds that frequently cap the MABL to estimate the lifting condensation level. Combining this information with radiometer-derived sea surface temperature measurements, an estimate of the near-surface moisture can be obtained to an accuracy of about 0.8 g kg^{-1}. Lidar-derived statistics on convective plume height and coverage within the MABL are then used to infer the profiles of potential temperature and moisture with a vertical resolution of 20 m. The rms accuracy of derived MABL average moisture and potential temperature is better than 1 g kg^{-1} and 1°C, respectively. The method relies on the presence of a cumulus-capped MABL, and it was found that the conditions necessary for use of the technique occurred roughly 75% of the time. The synergy of simple aerosol backscatter lidar and infrared radiometer data also shows promise for the retrieval of MABL moisture and temperature from space.

1. Introduction and background

The planetary boundary layer (PBL), ranging in thickness from less than 100 m to over 4 km, is the region of the atmosphere in direct contact with the earth's surface. The importance of the PBL to atmospheric dynamics and weather forecasting is well documented. Moisture and heat at the surface are transferred into the atmosphere within the PBL and are transported to other regions of the atmosphere mainly by turbulence and convective motions. Since the PBL contains a large percentage of the total atmospheric moisture, it determines to a large degree the amount of latent heat available to fuel deep convection and storm development. Over the oceans, the moisture content of the lower PBL is especially important because if the surface wind speed and sea surface temperature (SST) can also be measured, an estimate of the surface moisture flux can be made using bulk aerodynamic methods. The flux of moisture (as well as heat and momentum) from the sea surface to the atmosphere is very important for accurate weather and climate prediction as well as for driving ocean models (Chou and Atlas 1982; Chou et al. 1995). Evaporation over the tropical oceans may also play an important role in El Niño–Southern Oscillation (ENSO) episodes by producing anomolous cooling of the sea surface and heating of the atmosphere during an ENSO episode (Liu 1988).

Much work has been done over the last 20 years on the passive retrieval of total atmospheric column water vapor in both the infrared (IR) (Prabhakara and Dalu 1979; Schluessel 1989) and the microwave region (Liu

Corresponding author address: Stephen P. Palm, Code 912, Goddard Space Flight Center, Greenbelt, MD 20771.
E-mail: spp@virl.gsfc.nasa.gov

and Niiler 1984; Chang et al. 1984; Liu 1986) from space. More recently, the ability to derive crude vertical profiles of moisture and estimates of surface moisture over the oceans has been demonstrated (Wagner et al. 1990; Schulz et al. 1993; Schluessel 1989). Data from the Special Sensor Microwave/Imager (SSM/I) currently in earth orbit have been utilized to estimate the total column water vapor amount to better than 10% by noting the relationship between the observed microwave brightness temperature and the radiosonde-derived total column water vapor amount (Schluessel and Emery 1990). Further work by Chou et al. (1995) utilized empirical orthogonal functions (EOFs) also used by Liu (1986) relating the measured microwave brightness to the radiosonde-measured total column atmospheric moisture. Chou et al. (1995) and Schulz et al. (1993) have both successfully derived surface humidity over oceans with accuracies approaching 0.9 kg m^{-2}.

Because of the shallow depth and variability of PBL height, it is very difficult to use either passive IR or microwave remote sensing to infer the detailed temperature or moisture structure of the PBL from space. At present, the best spaceborne retrievals of atmospheric moisture yield vertical resolutions on the order of 1 km. More detailed vertical profiles of moisture or temperature within the PBL are simply not possible from space at present. Clearly, there is a need to develop new techniques that can adequately resolve the moisture and temperature structure of the PBL from space.

Ground-based and airborne lidars have for many years remotely measured the temperature and moisture structure of the troposphere, including the PBL with high spatial and temperal resolution. Differential Absorption Lidar (DIAL) techniques use multiple wavelength laser beams—one tuned to the frequency of a strong water vapor absorption line and another tuned to a nearby spectral region that is highly transparent. DIAL systems have flown on aircraft and have demonstrated high-resolution (200 m in the vertical and 2 km horizontal) measurements of water vapor that agree with observation to within 10% (Higdon et al. 1994). Another technique utilizes a very weak molecular scattering effect known as Raman scattering to derive water vapor concentration. Raman lidar uses a single wavelength laser and a dual wavelength receiver to detect the frequency-shifted Raman scattering from nitrogen and water molecules (Whiteman et al. 1992). However, the Raman backscatter cross section is very small, and many shots from a high-power lidar system must be averaged to retrieve the water vapor amount. Of the two approaches, the DIAL technique is more suited for spaceborne application, but an orbiting DIAL system is still years from reality.

A simple aerosol backscatter lidar has, on the other hand, already flown in space during the Lidar In-space Technology Experiment (LITE), and plans are under way for the launch of a long-term orbiting system by 2002 (Hartman 1994; McCormick 1995). The main uses of a spaceborne atmospheric backscatter lidar include cloud and aerosol profiling and retrieval of boundary layer height. If such a system is combined with a multichannel passive radiometer, it may also be possible to estimate surface moisture and profiles of moisture through the depth of the MABL over the ocean. We have developed a technique to remotely infer near-surface moisture and the temperature and moisture structure within the MABL over the tropical and subtropical oceans using airborne IR radiometer and ordinary aerosol backscatter lidar data. This new method has the ability to provide high vertical (20 m) and horizontal (50 km) resolution of MABL temperature and moisture structure and, most importantly, should be applicable to spaceborne lidar systems as well. In this paper we will discuss the technique and present the results of 16 moisture and temperature retrievals and compare them with dropsonde observations acquired from the aircraft in the same regions. Section 2 will present the experiment setting, and section 3 will detail the instruments used to acquire the data. The retrieval of near-surface mixing ratio from lidar and radiometer data will be described in section 4, and the vertical profiles of moisture and temperature in section 5. Section 6 summarizes and concludes the paper.

2. Experiment overview

During the fall of 1994, we participated in the LITE aircraft correlative measurement program that was designed to collect coincident lidar measurements along the shuttle flight track for LITE data validation and correlation. LITE, flown aboard the shuttle *Discovery* in September 1994, was the first atmospheric lidar to fly in space. A description of the LITE system and the type of measurements it is designed to make can be found in McCormick et al. (1993). While the main objective of the correlative aircraft campaign was validation of LITE data, other instruments were flown to complement our downward-looking lidar in order to investigate the MABL and its interaction with the ocean. Specifically, we were interested in studying how MABL height and structure respond to changes in SST and surface wind speed over the ocean.

A total of five flights were performed aboard the NASA P3-B aircraft over the tropical and subtropical Atlantic Ocean, each flight acquiring between 5 and 7 h of data covering on average about 2500 km. A map with the position and dates of the flight tracks is shown in Fig. 1. While LITE acquired a substantial amount of data during the daytime, all five correlative aircraft flights were planned as nighttime missions because data from the LITE instrument have the highest quality in the absence of sunlight. The instrumentation onboard the P-3B consisted of the Large Aperture Scanning Airborne Lidar (LASAL) system (Palm et al. 1994), the Radar Ocean Wave Spectrometer (ROWS) system (Vandemark et al. 1994), the NASA/JPL Sea Surface Tem-

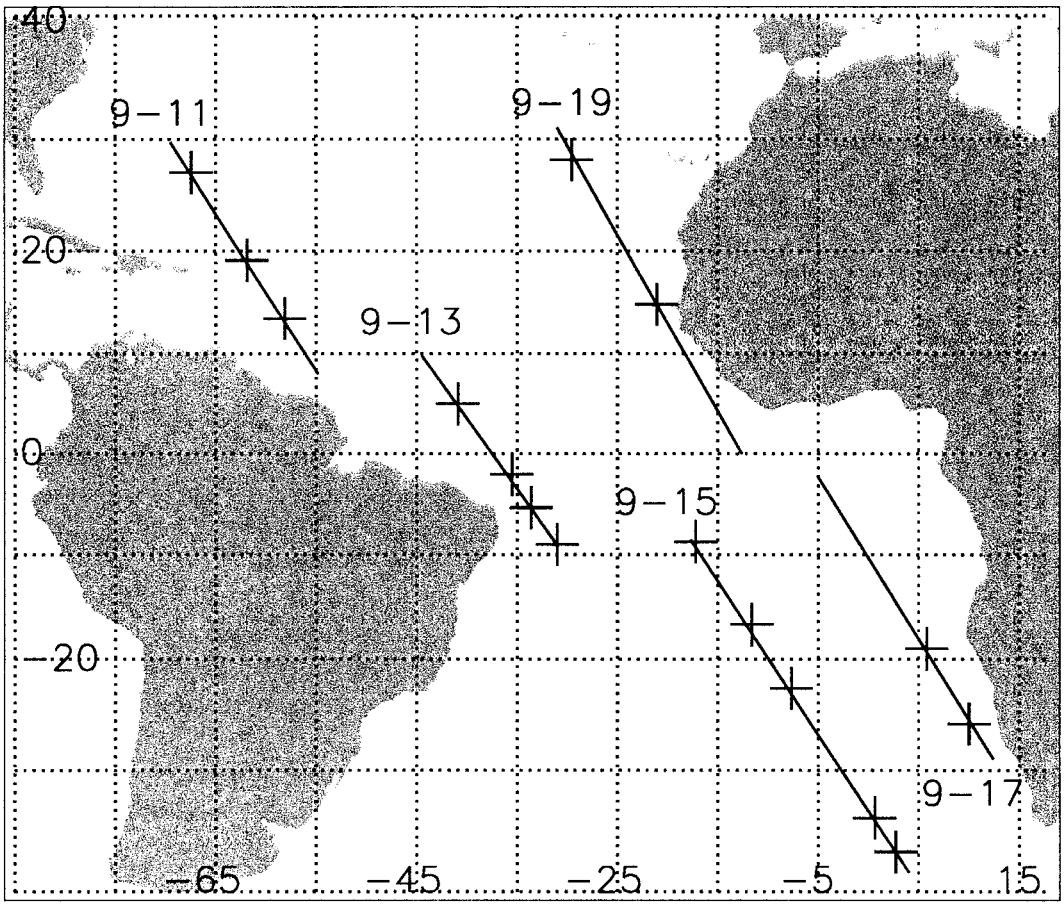

FIG. 1. P-3B flight tracks for the five LITE underflights with positions of dropsonde launches indicated by "+".

perature Radiometer (SSTR) (Hagan 1988), and the University of Massachusetts Ku-band scatterometer (KUSCAT) (Carswell et al. 1994). In addition, a dropsonde system was used to measure temperature, wind, and moisture profiles from the plane to the surface at intervals of about 400 km along the flight track. The position of each of the 16 dropsonde launches is shown as a "+" in Fig. 1. Data from ROWS and KUSCAT are not utilized in this paper. The following section will describe in more detail the three instrument systems used to acquire the data.

3. Instrumentation

a. Large aperture scanning airborne lidar (LASAL)

The LASAL instrument is a nadir viewing, scanning Nd:YAG-based lidar developed at NASA/Goddard Space Flight Center (GSFC) to probe the aerosol structure of the lower atmosphere. The system includes a large (36 in. × 25 in.) mirror, having two axes of motion, mounted underneath the laser table (in the bomb-bay section of the NASA P-3B aircraft). It is capable of scanning 45° left and right of the aircraft flight track (across track) and up to approximately 40° fore of nadir along the flight track. LASAL can render the three-dimensional structure of the convective boundary layer and derive optical thickness over large areas. In the across-track scan mode, measurements are made of attenuated aerosol backscatter cross section with emphasis on the structure, height, and organization of convection within the PBL. In the along-track mode, aerosol optical depth from backscatter at various angles from the same scattering volume is measured. LASAL was first integrated into the NASA WFF P-3B aircraft in 1990 and successfully operated in both scan modes (Palm et al. 1994). Since that time, and in preparation for the LITE correlative underflights, LASAL was modified to increase its capabilities. A new 50-Hz high-energy laser (550 mJ per pulse) was purchased to enable LASAL to substantially increase its horizontal resolution while also scanning at a higher rate. A new receiver optics package, including a new avalanche photo diode (APD) detector, was installed, and a new high-speed data system was designed and assembled. These enhancements significantly increased LASAL's performance as measured by signal-to-noise ratio and data resolution. During the LITE underflights, LASAL was operated in both the scanning and nadir-viewing modes. The nadir-pointing

mode of LASAL is utilized to obtain a very high horizontal resolution (3 m) of the MABL structure and height.

b. Sea surface temperature radiometer (SSTR)

The NASA/JPL SSTR is a multispectral, IR radiometer that operates in the down-looking mode. The radiometer, whose calibration characteristics are described elsewhere (Hagan 1988), is a six-channel, filter-wheel radiometer with a field of view of 1 mrad and a collecting aperture of 20 cm. Modulated radiance is focused by a Cassegrain telescope on to a liquid nitrogen-cooled HgCdTe detector. Interference filters define the optical bandpasses: two spectral regions, approximately 80 wavenumbers wide and centered at 860 and 940 cm^{-1}, and four contiguous spectral regions between 40 and 50 wavenumbers wide that cover the interval between 825 and 1005 cm^{-1}. The two wide bandpasses nearly match the 11- and 12-micron channels used by the Advanced Very High Resolution Radiometer (AVHRR), and the four more narrow bandpasses further subdivide the window region. The precision of the radiometer is 0.006°C for data acquired at 1 Hz, and the absolute calibration accuracy of the instrument is 0.07°C. The radiometer views the ocean through a germanium window whose temperature was monitored by internal and external platinum resistance temperature (PRT) sensors accurate to 0.01°C. The PRT readings are used to correct the detected radiance for the contribution by the window emission.

Sea surface temperature estimates are derived by regression of the brightness temperature measurements obtained in the four narrow optical bands. The technique is an extension of the method of Prabhakara et al. (1974). The regression relations, which differ for tropical and subtropical regions, were determined empirically from an extensive series of SSTR observations obtained during recent climate experiments, such as the Tropical Ocean and Global Atmosphere Coupled Ocean–Atmosphere Response Experiment (TOGA COARE) and the Central Equatorial Pacific Experiment (CEPEX). High accuracy in situ water vapor measurements were obtained simultaneously with the SSTR radiance profiles, and the effects of water vapor on the accuracy of SST retrievals are discussed in Hagan and Rogers (1997). A similar regression approach for deriving water vapor content is being developed following the method of Dalu (1986). Derived SST accuracies are on the order of 0.2°C.

c. Dropsonde

The NASA P-3B carried a total of 25 Lightweight Omega Digital Dropwindsondes (LOD2) for use during the LITE underflights. The LOD2 measures wind speed and direction, temperature, relative humidity, and pressure as it falls to the surface on a parachute at an average speed of about 8 m s^{-1} (Hock and Cole 1991). The data are radioed back to the aircraft at a rate of 4 Hz and stored on hard disk for future analysis. This gives a vertical resolution of the thermodynamic data of about 2 m. The resolution of the wind speed and direction is much less (about 200 m) because vertical averaging of the sonde position data is necessary to derive the wind vectors. The profiles are displayed in real time using a laptop PC as they are acquired.

The temperature sensor is a standard Fenwal 60-mil chip thermistor with a lead-carbonate coating. The accuracy of the sensor is about 0.5°C over the range from −55° to 40°C. Time constants for the temperature sensors have been evaluated and determined to be a function of altitude. At 550 mb (the P-3B flew at about 400 mb), the time constant is about 4.0 s, while at the surface it is roughly 2.5 s. The time constant of the sensor combined with the fall rate of the sonde produces a slight lag in the temperature measurement throughout the sounding. This problem is most severe when the sensor crosses large temperature gradients such as inversions normally present at the top of the PBL.

The humidity sensor is comprised of a heated alumina substrate with a thin deposit of a proprietary, carbon-based sensing material that changes its electrical resistance with changes in humidity. The time constant is less than 1 s and measurement accuracies of ±5% for $0°C \leq T \leq 56°C$ and ±8% for $-20°C \leq T \leq 0°C$ for the humidity range from 5% to 100%. The LOD2 utilizes a silicon-based piezo-resistive integrated pressure sensor manufactured by Sensym. It is internally temperature compensated and provides pressure to ± 2 mb. For further details regarding the dropsonde instrumentation, see Hock and Cole (1991).

4. Surface mixing ratio computation

The value of the surface mixing ratio over the oceans is extremely important because it partially governs the amount of latent heat flux from the ocean to the atmosphere. Over the Tropics and subtropics, where the sea–air temperature difference is generally very small, the magnitude of the latent heat flux is much larger than the sensible flux. Normally, for the computation of latent heat flux using the bulk aerodynamic method, wind speed and water vapor amount at the 10-m height are used. As a matter of convention, from here on when we speak of ''surface moisture'' or ''surface mixing ratio,'' we mean the value of the mixing ratio at the 10-m height, which is denoted herein as q_0. Also, we define the well-mixed layer of the MABL to denote the layer from the surface to the height of the lifting condensation level (LCL). The algorithm to retrieve surface mixing ratio initially derives a ''bulk'' water vapor amount applicable to the lower few 100 m of the MABL (q_b). This value is then adjusted to estimate q_0 as will be described in section 4b. Before continuing, we would like to dis-

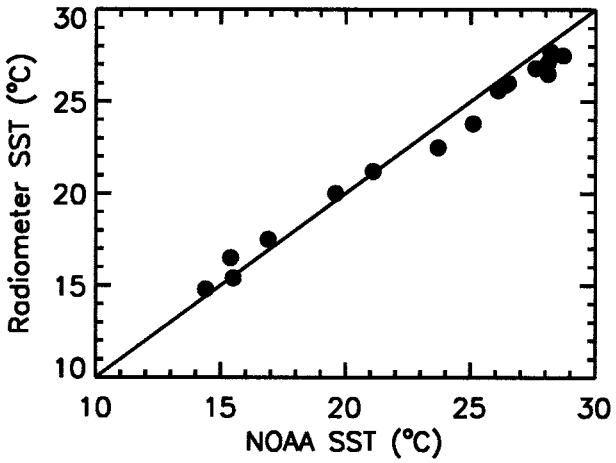

FIG. 2. A comparison of the NOAA and SSTR radiometer sea surface temperatures at the locations of the dropsonde launches. The NOAA values are weekly averages interpolated to the dropsonde location. The SSTR data is an average over about 10 km.

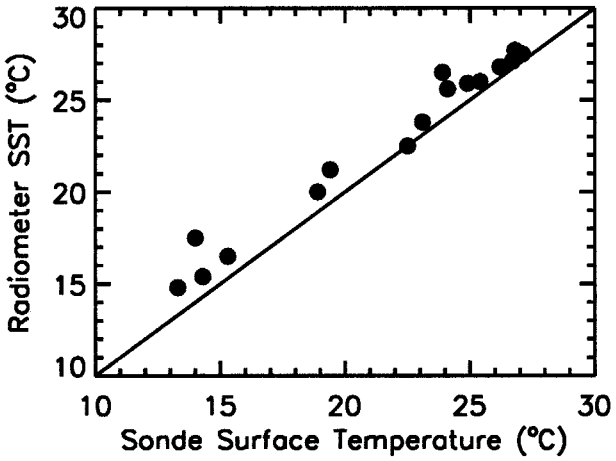

FIG. 3. A comparison of the SSTR-derived sea surface temperature values with the average dropsonde air temperature from the surface to 10 m.

cuss in detail the retrieval of SST because it is crucial to the success of the surface mixing ratio estimate.

a. SST measurements

The multichannel radiometer used on the P-3B has previously flown in the TOGA COARE campaign, as well as in other research experiments. Its ability to accurately measure SST is well documented from those campaigns. Other sources of SST data could be used such as the National Oceanic and Atmospheric Administration's (NOAA) weekly SST analysis, but it is not likely that they would be as accurate as the SSTR measurements. We are, however, compelled to present a comparison of the SSTR data with the NOAA SST to demonstrate consistency. In Fig. 2 we plot the SSTR-measured sea surface temperature versus the NOAA weekly average SST for the 16 dropsonde points. The NOAA SST values were linearly interpolated from the nearest grid point to the dropsonde location. The SSTR values were obtained as close to the dropsonde point as possible, but there were cases where clouds or lack of data prevented exact collocation. In general, the SSTR values were retrieved from data collected within 100–200 km of the dropsonde point. Figure 2 indicates good agreement between the SSTR sea surface temperature and the NOAA estimate. The bias is less than a half of a degree. Because of space and timescale differences in the two datasets, it is not expected for the NOAA and SSTR values to agree exactly. The locations, date, and time of the 16 dropsonde launches are listed in Table 1. Also shown is the SSTR-derived SST corresponding to each dropsonde location.

Another check on the SST values can be provided by plotting their values versus the surface temperature as measured by the dropsonde, which is shown in Fig. 3. The dropsonde-measured surface temperature is defined as the average of the lower 10 m of the atmosphere. This corresponds to the average of about five discrete

TABLE 1. Date, time, location, and SST for the 16 dropsonde launches.

Drop number	Date	Time (UTC)	Latitude	Longitude	SST (°C)
1	11 September	0437	27.12	−65.45	27.5
2	11 September	0621	19.12	−59.41	27.1
3	11 September	0730	13.49	−56.14	27.7
4	13 September	0322	5.00	−37.56	26.5
5	13 September	0446	−2.05	−33.52	26.0
6	13 September	0526	−5.36	−31.61	25.9
7	13 September	0609	−9.00	−29.50	25.6
8	14 September	2230	−8.71	−15.60	22.5
9	15 September	0009	−16.73	−10.67	21.2
10	15 September	0117	−22.70	−6.65	20.0
11	15 September	0317	−34.07	2.63	15.4
12	15 September	0347	−36.84	5.44	14.8
13	17 September	0000	−25.91	12.01	16.5
14	17 September	0125	−19.71	7.58	17.5
15	19 September	0051	14.87	−19.08	26.8
16	19 September	0339	28.32	−28.55	23.8

dropsonde temperature values. The averaging was not really necessary since very little gradient of temperature was seen in the lower 10 m of the dropsonde data. The calculated bias is −1.2°C, which is within the expected range (−0.5° to −1.5°C). Based on the general agreement of the SSTR-measured sea surface temperatures and the NOAA estimates, as well as the consistency with the dropsonde-measured surface temperature, we conclude that the SSTR is retrieving accurate SST values. The agreement between the SSTR-derived and NOAA SST values is such that the latter could have been used in place of the SSTR data without radically affecting the overall results of the lidar moisture retrievals presented in the following sections.

b. Lidar retrieval of cloud base height

In addition to SST, the other parameter needed to estimate near-surface moisture is the height of the LCL. While this cannot be measured directly, we can use cloud base height (CBH) as a good estimate for the LCL. From lidar measurements of fair weather cumulus clouds over land, Stull and Eloranta (1983) have demonstrated that the height of cloud base is a very good measure of the LCL when the latter is computed from surface measurements of temperature and dewpoint. Their measurements of CBH were obtained with a ground-based lidar system, but it is reasonable to expect that their results will apply to oceanic boundary layer clouds as well. Since the P-3B is flying well above the cumulus cloud tops, we cannot measure CBH directly but rather must infer or estimate the CBH based on the measurement of cloud-top height. The technique we have developed will work through a large range of approximately 10%–90% cloudiness. It will obviously neither work in totally clear conditions nor work in areas of complete cloud cover. Typically, over large areas of the tropical ocean, the MABL is capped by cumulus clouds, which are frequently within this 10%–90% cloudiness range. Of the 21 dropsonde launches during the LITE underflights, we were able to estimate CBH 16 times, or approximately 75% of the time. Three of the dropsonde launches occurred over solid stratus cloud cover and two others occurred in regions of tall convective clouds. In these areas, no retrievals can be made. The basic algorithm for determining CBH from the lidar data is as follows.

- Find all cloudy lidar shots for a segment of data roughly 50 km in length.
- Locate the top of the cloud for each shot from the lidar backscatter profile.
- Construct a histogram of the cloud-top heights.
- Choose the CBH as that height where 95% of the cloud tops are above that level and 5% are below.

Cloud-top heights must be used in the estimation of CBH since directly sensing cloud base from above the clouds using lidar is difficult and limited to optically thin clouds. Direct sensing of CBH may work for some clouds provided that the optical depth of the cloud is small enough such that the lidar return is not totally attenuated before reaching cloud bottom and that the lidar signal detector does not suffer saturation from the large signal experienced at cloud top. This method was not utilized here but may prove useful under certain conditions.

The technique developed for CBH detection from cloud tops has its basis in the idealized shape of a cumulus cloud. Casual observation of daytime, fair weather PBL cumulus clouds reveals that often one side of the cloud is sloped from a more narrow top to a wider base. This is indicative of the presence of wind shear in the entrainment zone, and the upward-sloping edge of the cloud will always point in the direction of the shear. For such a cloud, the lowest cloud-top height will be very close to (although slightly above) actual cloud base height. The procedure to measure cloud top height from the lidar data is summarized below.

The lidar data are processed somewhat differently according to the acquisition mode. For data acquired in the fixed nadir-pointing mode, 10 shots are averaged together producing a horizontal resolution of about 30 m. For data taken in the across-track scanning mode, two nadir shots are stripped from the scan sequence and averaged. This results in a horizontal resolution of about 350 m for a scan rate of 60° s^{-1} and aircraft velocity of 120 m s^{-1}. It is possible to use the scan data from angles other than nadir for cloud base detection, and indeed there are times when this might be advantageous, but we have decided not to do so for two reasons. First, it gives us an opportunity to access the impact of data resolution on the retrievals, and second, the same set of algorithms can be applied to the data regardless of how the data were acquired, rendering more consistency in the data analysis. LASAL was operated in the across-track scan mode on 11 and 17 September. The other three days (13, 15, and 19 September) LASAL was operated in the nadir-pointing direction. Prior to averaging, the backgound is subtracted from each shot, and range correction is applied. Each averaged profile is then examined to find the ground return. It is crucial to the technique to be able to discern between a clear return and one from a cloud. Fortunately, for most lidar data differentiating between clear and cloudy returns is quite easy. When a cloud is encountered, it will attenuate the laser beam and, depending on the optical depth of the cloud, will either partially or totally attenuate the signal return below the cloud. This will result in either no ground return or a very weak ground return below clouds. This attenuation is easily recognized upon close inspection of the lidar return profile. A return is classified as cloudy if the ground return value is less than half of the maximum or saturated return signal. Next, the shot is examined to locate the cloud top by starting well above the MABL top (2.5–3.0 km) and searching downward for a rapid increase and then saturation in

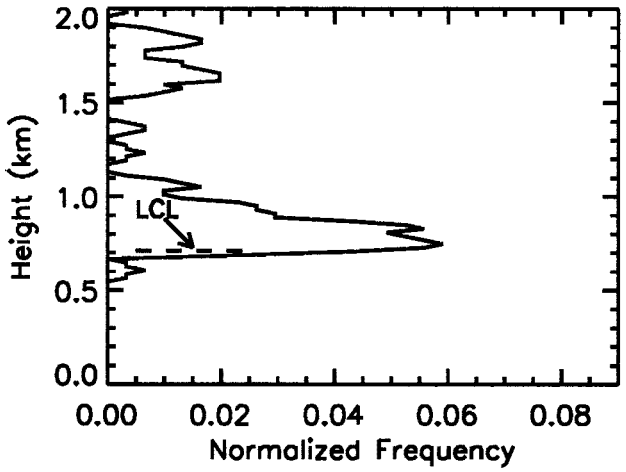

FIG. 4. Histogram of cloud-top heights with the estimated lifting condensation level (LCL) shown as dashed line.

return signal. Clouds will usually saturate the detector, but saturation is not a prerequisite for the presence of a cloud. The point just before reaching saturation (or maximum signal) is assumed to be the top of the cloud. The height of the cloud top is then calculated based on the position of this range bin and the position of the last ground return range bin. This process continues for 50 km or so of data, and then the cloud-top height data are binned into intervals 20 m wide, producing a histogram of cloud-top height, as in Fig. 4.

The lowest cloud heights in this histogram are those most closely associated with cloud base. We have found from previous experience in the Frontal Air–Sea Interaction Experiment (FASINEX) that the 95% level on the cloud-top frequency curve (that level where 95% of the cloud tops are above and 5% of the cloud-top heights are below) correlates very well with the LCL. The 95% level is shown as the dashed line in Fig. 4. We checked the accuracy of this method by using the dropsonde data to compute the LCL and found an rms error of 160 m with a bias of about 50 m. This indicates that the lidar estimate of LCL is, on average, too high and that the inaccuracy in LCL determination will introduce an error of about 7%–8% into the estimation of surface mixing ratio (see Fig. 5a). Errors in the estimation of the surface air temperature will either add to or subtract from this error, depending on whether it is under- or overestimated. This is discussed further in the next section.

c. Surface moisture computation

After the LCL is found from the histogram of the cloud-top heights, the corresponding temperature and pressure at the height of the LCL is computed from an estimate of the surface pressure and temperature. We assume that the surface air temperature is 0.8°C cooler than the sea surface temperature for all cases. The air–sea temperature difference of −0.5° to −1.2°C is typical

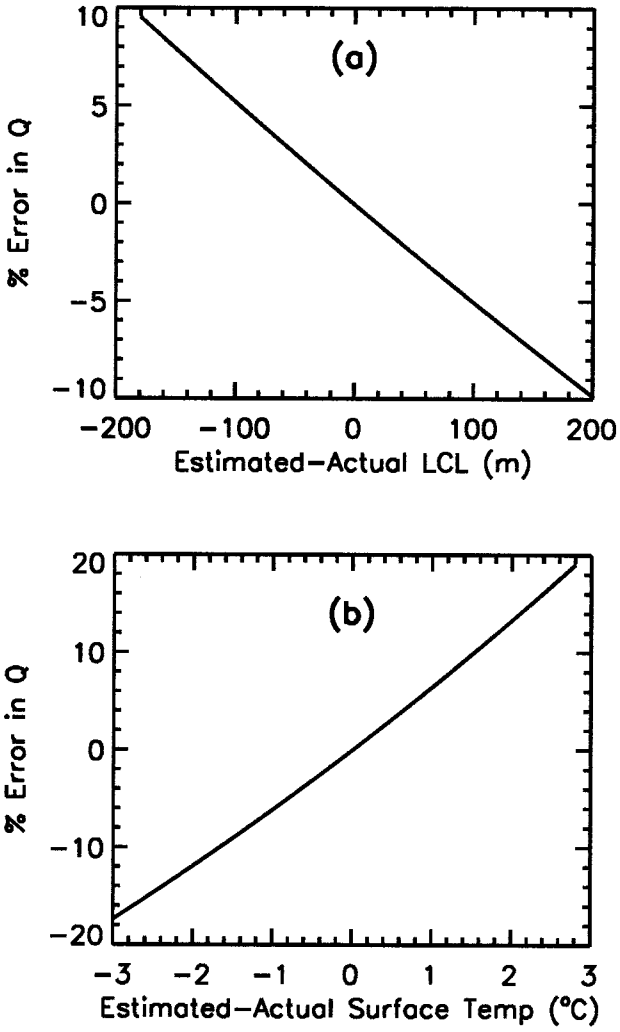

FIG. 5. The percent error in computed surface mixing ratio values as a function of errors in lifting condensation level (LCL) and (a) surface air temperature (b) assuming a perfectly well-mixed boundary layer up to the height of the LCL.

of air over the ocean in the Tropics and subtropics (provided sufficiently far from land), and similar values were seen during the TOGA COARE and CEPEX campaigns in the equatorial Pacific Ocean (Webster et al. 1996) and during FASINEX in the subtropical western Atlantic Ocean (Weller et al. 1995). There may be diurnal effects on the SST, especially in a relatively calm sea state, but since all of our data were gathered at night, we cannot evaluate these effects. In general, we expect the sea–air temperature difference to be larger during the day than at night.

The correct measure of the surface air temperature is crucial to the accuracy of the final mixing ratio estimate. Theoretically, a 1°C error in surface temperature will produce a 10% error in the retrieved surface mixing ratio. The surface pressure is assumed available from synoptic charts or recent numerical model initial field

analyses. The retrieval of mixing ratio is not sensitive to surface pressure errors, with an 8-mb resulting in only a 1% error in retrieved mixing ratio. The impact of errors in estimated surface temperature and LCL on the final retrieval of q_0 is shown in Fig. 5. The sensitivity of q_0 on LCL errors is minimal. If we are within 100 m of the actual LCL, the induced error in retrieved mixing ratio will be no greater than about 5%. This is fortunate, as the technique to estimate LCL from the distribution of cloud tops shows an error of this magnitude. Another source of error results from the degree to which the layer from the surface to the LCL deviates from the well-mixed assumption. This error is generally small but could be appreciable over areas of cool SST and especially where the SST is less than the air temperature.

The temperature at the height of the LCL (T_s) is computed by assuming that the temperature lapse rate from the surface to the LCL is adiabatic. The pressure at the LCL (P_s) is derived from the hypsometric formula using the average of the temperature at the LCL and the surface temperature as the mean temperature of the layer. Once the temperature and pressure of the LCL have been estimated, the saturation mixing ratio (q_s) in grams per kilogram at that temperature and pressure is calculated using the standard formula

$$q_s = \frac{622e_s}{P_s - e_s} = q_b, \tag{1}$$

where e_s is the saturation vapor pressure at T_s. The saturation mixing ratio at the LCL is equivalent to the actual mixing ratio at the surface, assuming that the MABL is perfectly well mixed (no gradients of mixing ratio) from the ground to the LCL. While this is not always the case, the gradients that usually exist are relatively small. In actuality, the value of mixing ratio that is derived from this procedure is more representative of the bulk moisture content of the layer between the surface and the LCL. We call this value q_b. Because there is often a gradient of moisture within the surface layer of the MABL, we estimate the surface mixing ratio (q_0) to be 4% higher than q_b as

$$q_0 = q_b 1.040. \tag{2}$$

The value of 4% was chosen based on the observed behavior of the dropsonde mixing ratio in the lower 100 m of the MABL.

Figure 6 presents the results of the surface mixing ratio computation for the 16 retrieval cases plotted against the dropsonde observation. The rms error is 0.8 g kg^{-1} or about 7% of the average observed surface mixing ratio value (11 g kg^{-1}). The agreement is quite good. The magnitude of the rms error is consistent with the expected error that is introduced by inaccurate LCL determination, as discussed in section 4c. There is little apparent overall bias to the retrievals, but it appears that q_0 is generally underestimated over cold ocean water (which corresponds to the lowest observed q_0 values) and overestimated over warm water (highest observed q_0 values). This might be indicative of the sensitivity of the retrieval on surface air temperature. Possibly, the assumed sea–air temperature difference of 0.8°C is a weak function of sea surface temperature. If the sea–air temperature difference is in reality less over cooler water and larger over warm water, the effect on the moisture retrieval would be consistent with the results shown in Fig. 6 (overestimate q_0 over the warmer water and underestimate q_0 over cool water). The data in Fig. 3, however, do not seem to substantiate this and in fact seem to show a slight increase in sea–air temperature difference as radiometric SST decreases. A more likely explanation might lie in the stability of the MABL. Over cold water it is likely that the MABL is more stable than over warm water. Higher stability will in general make the well-mixed assumption less valid and thus adversely affect the resulting mixing ratio retrieval.

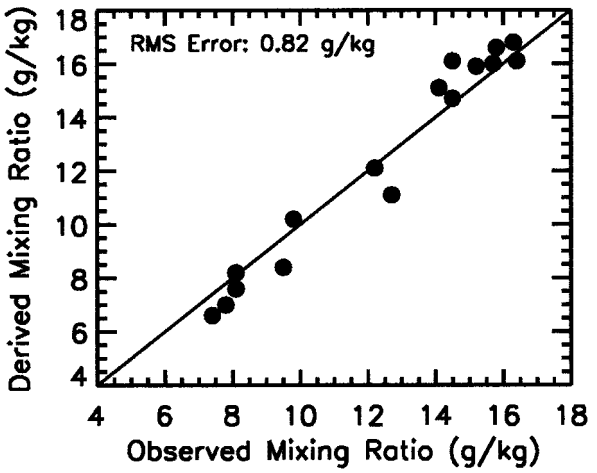

FIG. 6. Dropsonde-observed vs lidar-derived surface mixing ratios (q_0) for all 16 retrievals.

5. Vertical profiles of moisture and temperature

In this section, we present a technique to infer vertical profiles of moisture and temperature in the MABL based on the SST measurements and the surface mixing ratio estimates derived in the previous section. The derivation of temperature and moisture profiles using the lidar data requires that we construct a histogram of the vertical distribution of aerosol gradients within the MABL; the rationale being that aerosol gradients seen in the lidar data are actually the edges or boundaries of convective cells that originate in the well-mixed layer and rise an arbitrary distance before becoming neutrally buoyant. At any given height, the moisture and temperature of the air depend to a great extent on the number of times parcels originating in the well-mixed layer have penetrated through the weak inversion at cloud base and deposited their mixed layer properties into the cloud layer. This is where the utility of the lidar measurement

comes in. As long as the parcels that originated in the mixed layer and have broken through to the cloud layer can be identified using their aerosol backscatter signatures, then we can in effect develop a histogram that tells us the percentage of time this has occurred as a function of height and therefore how much the cloud layer has been modified by mixed layer parcels. It is well documented that aerosol backscatter lidar provides a means of detecting the top of the boundary layer by sensing the increased backscatter associated with the higher aerosol concentrations (as well as higher humidity) within the boundary layer (Melfi et al. 1985; Sasano 1984; Boers et al. 1984; Kaimal et al. 1982). Further, it has been shown that lidar can detect upward-rising convective plumes within the boundary layer and distinguish these from areas of entrained, clearer, and drier air from above the MABL (Melfi et al. 1985; Ferrare et al. 1991). It is acknowledged that under conditions of very low surface flux, when convective cells within the MABL may not be very well defined, it may be very difficult to distinquish a convective cell boundary based on its gradient of backscatter between it and the ambient MABL air. However, our experience during the LITE aircraft campaign and previous airborne lidar experiments [such as the Genesis of Atlantic Lows Experiment (GALE 1986), the Convective Wave Experiment (COWEX 1990), and FASINEX 1986] indicates that these conditions occur infrequently over the ocean.

a. Method

Each lidar profile is searched from the ground upward for substantial gradients in backscatter that are indicative of the boundaries of convection cells or plumes. This is done with a computer algorithm that searches for vertical gradients of backscatter that are greater than a certain threshold level. The procedure is similar to the one detailed in Melfi et al. (1985) for the detection of boundary layer height from airborne lidar data. However, instead of searching for only one large gradient (the MABL top), this algorithm searches for all aerosol gradients from the ground to the MABL top. A number of these aerosol gradients may occur through the depth of the MABL for the same lidar shot and the algorithm searches for a maximum of five. Typically, two or three aerosol gradients are found per lidar return with five being very rare. A height is assigned to each of the aerosol gradients, and this procedure is repeated for each lidar shot of the 50-km data segment surrounding the dropsonde launch point. The heights of the aerosol gradients are then binned into intervals 20 m wide (the vertical resolution of the lidar data is 15 m) to form a histogram similar to Fig. 4. Letting $H(z)$ represent the histogram of aerosol gradient heights and Z denote the height where $H(z)$ goes to zero at the MABL top (the height of the highest detected aerosol gradient), we define the cumulative probability distribution of detected aerosol gradients [$P(z)$] as

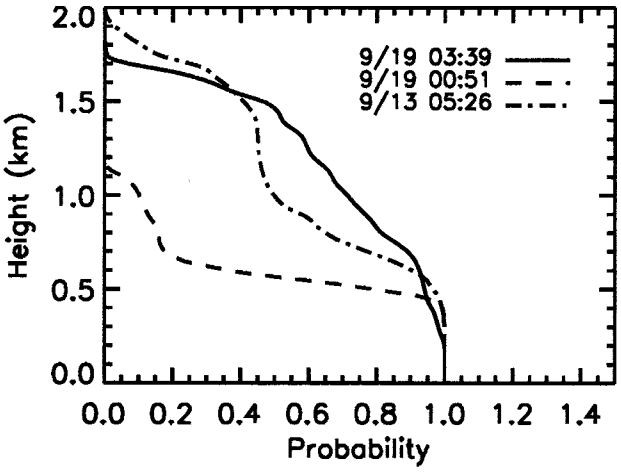

FIG. 7. Probability of well-mixed layer air reaching a given altitude for three retrievals.

$$P(z) = 1.0 - \frac{\sum_{z=0}^{z} H(z)}{\sum_{z=0}^{Z} H(z)}. \qquad (3)$$

Shown in Fig. 7 is the cumulative probability distribution of detected aerosol gradients for three cases. Physically, it can be thought of as representing the percentage of time that air from within the well-mixed layer reaches a particular height. The air below the lowest detected convective cell heights (about 200 m for the 0339 UTC 19 September case) is always within the well-mixed layer. If one were to take a horizontal slice through the MABL at this height, air from the free troposphere above would never be encountered. Likewise, at the 1400-m height, where the frequency of occurrence is 50%, air from within the well-mixed layer would be expected to be found 50% of the time as would air from above the MABL. An estimate for the temperature or moisture at this level would be a weighted average of the properties of the air from within the well-mixed layer and the air above the MABL.

The resulting potential temperature and mixing ratio profiles are calculated as

$$q(z) = P(z)q_b + [1 - P(z)]q_t, \qquad z > h_{sl} \qquad (4)$$

and

$$\theta(z) = P(z)\theta_0 + [1 - P(z)]\theta_t, \qquad z \geq 0, \qquad (5)$$

where $P(z)$ is the normalized cumulative frequency distribution of aerosol gradients, q_b is the bulk MABL mixing ratio defined in (1), θ_0 is the surface potential temperature, and h_{sl} is the height of the surface layer. As in section 4c, θ_0 is assumed to be 0.8°C cooler than the SST potential temperature. Here, $q_t = 0.30q_0$ and $\theta_t = \theta_0 + 7.0$ are the estimated free troposphere values of mixing ratio and potential temperature, respectively. The potential temperature and mixing ratio values at the

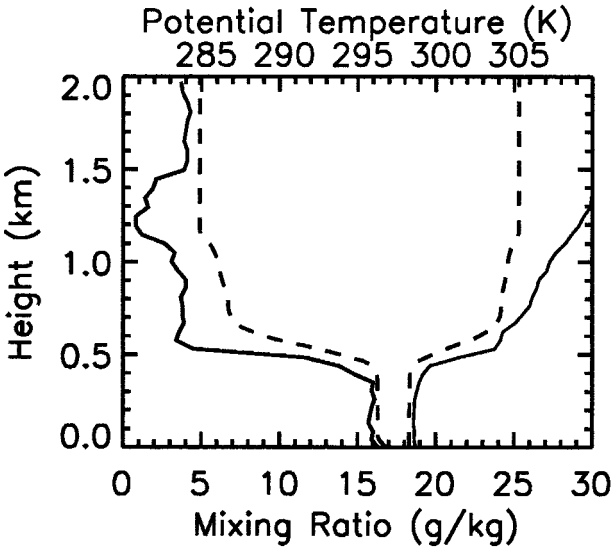

FIG. 8. Lidar-derived profiles of mixing ratio and potential temperature (dashed) shown with observed dropsonde profiles (solid) from drop 15, 0051 UTC 19 September 1994. The mixing ratio is on the left (lower axis) and potential temperature (upper axis) is to the right.

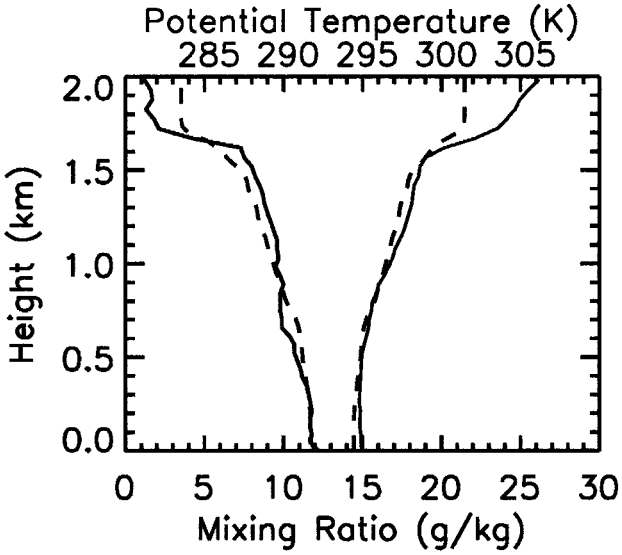

FIG. 9. Same as Fig. 8 except for drop 16, 0339 UTC 19 September 1994.

MABL top vary considerably in space and time, and these are simply best-guess values based on the observed dropsonde profiles. Improvement in the retrieved profiles could be obtained if more accurate estimates of q_t and θ_t from other sources were available. For the purposes of this paper, h_{sl} is taken to be 10% of the height of the lifting condensation level. From the surface to h_{sl}, the mixing ratio profile is linearly adjusted as

$$q(z) = q_0\left(1.0 - \frac{0.040z}{h_{sl}}\right), \qquad 0 \le z \le h_{sl}. \quad (6)$$

This adjustment is made to allow for the frequently observed gradients in q within the lower 50–100 m of the MABL (the surface layer). The magnitude of the moisture gradients in the surface layer depend on stability and sea–air temperature difference. Since we are assuming a constant sea–air temperature difference and a neutral lower MABL everywhere, a constant adjustment as in (6) is justified. For the heights above h_{sl}, the surface moisture and temperature values are weighted at each height level by the percentage of time the air at that level is either of mixed layer or free troposphere origin to obtain the estimated profiles.

In the following section, we present the profiles of MABL moisture and potential temperature for 10 of the 16 retrievals and compare them with the dropsonde measurements. We start with the last flight day (19 September) and work backward, showing two retrievals for each day.

b. Results and discussion

Figures 8 and 9 show retrieval results of MABL mixing ratio and potential temperature for dropsonde launches 15 and 16 on 19 September 1994 off the west coast of Africa. The solid lines are dropsonde observations and the dashed lines are the lidar retrievals. The θ profiles are plotted on the right with corresponding scale at the top, while the profiles of q are plotted on the left with corresponding scale on the bottom. The profiles are meaningful only for the heights where $P(z) > 0$. The height where $P(z)$ goes to zero represents the top of the MABL, as defined by the lidar data. Thus, in Fig. 8, above 1.2 km the profiles attain the constant value of q_t and θ_t because there are no statistics on plume distribution above that height. As was mentioned in section 3, roughly 50 km of cloud and MABL height statistics must be gathered to ensure accurate LCL determination. The lidar data were chosen such that the dropsonde launch occurs in the center of the 50-km lidar data segment. It should be recognized, however, that the dropsonde profile represents a point measurement, whereas the lidar-derived profile is a spatial average, which in some respects is more representative of the MABL than a single dropsonde measurement. Because of this, it is quite possible to have fairly substantial differences in the shape of the profiles, especially in the region of the entrainment zone (upper 10%–20% of the MABL). For instance, if the dropsonde happened to fall through a convective cell that was penetrating to the upper reaches of the entrainment zone, then the inversion would appear higher and stronger than if the sonde had fallen in a region between convective cells. This could at least partially explain the lower inversion as measured by the dropsonde in Fig. 8 compared to the lidar-estimated profile. Additionally, the time lag of the temperature sensor, as discussed in section 3c, could induce errors in the observed profile, especially at the height of the strong inversion capping the MABL. The

TABLE 2. Observed and retrieved surface moisture (q_0), average moisture ($\bar{q}$), and potential temperature ($\bar{\theta}$) for the entire depth of the MABL.

Drop number	Obs q_0	Ret q_0	Obs $\bar{q}$	Ret $\bar{q}$	Obs $\bar{\theta}$	Ret $\bar{\theta}$
1*	15.8	16.6	14.5	15.0	299.2	299.6
2*	15.2	15.9	12.2	12.7	300.0	300.3
3	14.5	16.1	11.3	11.6	301.1	301.3
4	16.4	16.1	14.6	13.4	299.8	298.3
5	15.7	16.0	11.8	12.0	301.1	299.2
6*	14.5	14.7	10.7	10.4	299.3	299.8
7*	14.1	15.1	11.1	11.9	298.9	298.6
8*	12.7	11.1	9.7	8.3	296.5	295.7
9	9.8	10.2	8.9	8.7	291.3	293.2
10	9.5	8.4	7.2	6.0	291.3	293.2
11	7.4	6.6	5.4	4.5	290.0	289.9
12*	7.8	7.0	5.9	5.2	288.5	288.4
13*	8.1	7.6	6.7	6.0	288.8	289.3
14*	8.1	8.2	7.2	7.1	288.3	289.6
15*	16.3	16.8	15.3	16.3	299.0	298.3
16*	12.2	12.1	9.9	9.8	296.5	296.1
Rms error	0.81 g kg^{-1}		0.73 g kg^{-1}		0.81 K	

* Indicates that the profiles for this retrieval are shown and discussed in the text.

descending dropsonde will ''remember'' the cooler air temperatures above the inversion top and thus tend to measure a lower inversion height (Skony and Kahl 1994). Even considering these factors, the retrieved profiles of moisture and temperature for 19 September are remarkably good. The overall shape of the profiles match the observations quite well.

Figure 9, based on data acquired at about 28°N, shows the best agreement with observation of the 16 retrievals with the average MABL moisture content agreeing with the dropsonde to within 1% (see Table 2). The potential temperature profile retrieval for this case is also very good up to the capping inversion at 1.6 km. As a matter of fact, one might be inclined to state that the agreement between observation and retrieval in Fig. 9 is too good since we are comparing an instantaneous measurement with a spatial average. The degree to which the point measurement of a dropsonde will vary from a spatial average over 50 km depends on the magnitude of the variance of temperature and moisture within the MABL. Over the open ocean, and assuming little change in SST over a distance of 50 km, the MABL will be in near equilibrium with the underlying surface provided there are no weather disturbances or fronts in the area. Under these conditions (which apply to the data presented here), the variance of temperature and moisture within the MABL will be relatively small. The aircraft observations of Warner and Telford (1967), Grant (1965), and Lenschow (1970), over both water and land, show that the magnitude of temperature and moisture fluctuations within the atmospheric boundary layer are between 0.5° and 1.5°C and 0.5 and 1.6 g kg^{-1}, respectively. In addition, their findings indicate that the greatest deviation from ambient conditions occurs in the lower few hundred meters of the boundary layer and also at and slightly above cloud base with a distinct minimum in variance in both temperature and moisture at about 500 or 600 m. The results of Konrad and Robison (1973) indicate that the fluctuations of temperature and moisture within a developing boundary layer over land can approach 3°C and 5 g kg^{-1}, respectively. Most of their results, however, were more in line with the magnitudes reported by Grant (1965). Additionally, they find that variations of temperature and moisture are greatest within the entrainment zone near the top of the boundary layer. These investigations all used data that was acquired over land in late spring or summer on sunny days. Such conditions are probably more conducive to higher temperature and moisture variance due to the strong solar heating producing larger land–air temperature differences and greater surface fluxes than is typical over the tropical ocean. This leads to the conclusion that the variance of moisture and temperature within the MABL in our flight regions was probably less than 1.0 g kg^{-1} and 1.0°C, respectively, and further that these would be the likely magnitude of differences noted between a dropsonde point measurement and a 50-km spatial average measurement. Differences of this magnitude between dropsonde observation and the retrieved profiles are seen throughout the data presented in this paper.

Figures 10 and 11 show the retrievals for the flight from Capetown, South Africa, to Ascension Island on 17 September 1994. During the first half of this flight, we encountered the coldest SST of the LITE campaign. This is not surprising given the fact that winter is just ending and we are flying over relatively shallow shelf waters close to the African coast. Figure 10 (drop 14) is based on data acquired at about 19°S and shows a very stable boundary layer over cool ocean water. In fact, this sounding was acquired just at the edge of an extensive stratocumulus cloud deck that extended from 18°S to about 4°S along the flight track. Comparison of

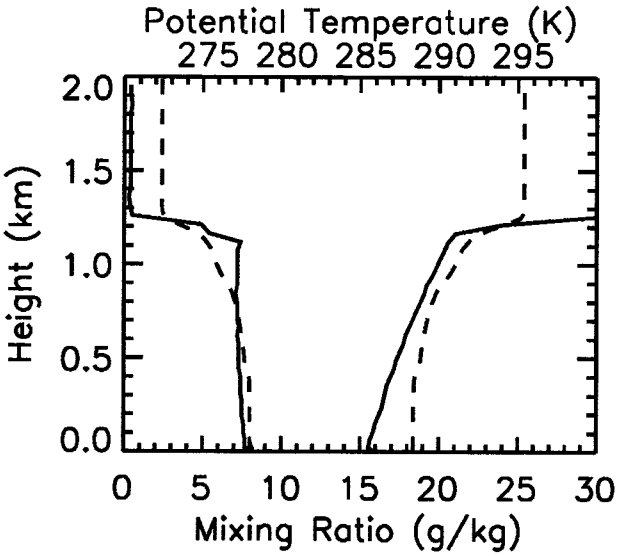

FIG. 10. Same as Fig. 8 except for drop 14, 0125 UTC 17 September 1994.

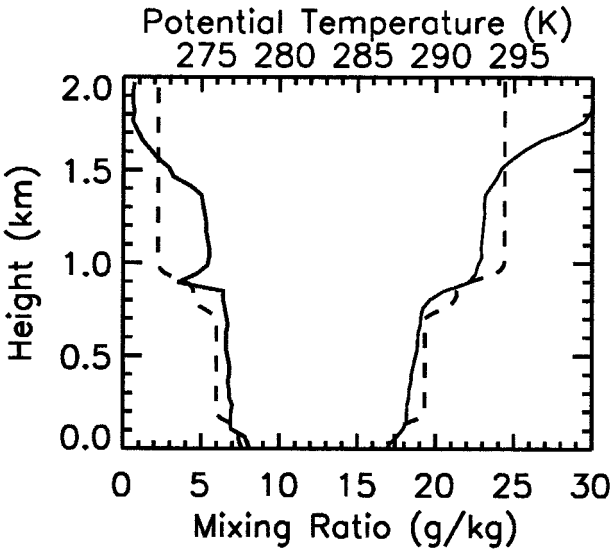

FIG. 11. Same as Fig. 8 except for drop 13, 0000 UTC 17 September 1994.

the observed and retrieved potential temperature indicates that the air temperature close to the surface was considerably cooler (about 3°C) than the sea surface temperature (recall that the retrieved surface potential temperature is set to 0.8°C less than the sea surface potential temperature). This could be due to the proximity of the coast or possibly the effect of the nearby stratus deck. This was the largest sea–air temperature difference seen during the entire mission. It is interesting to note that this relatively large error in estimated surface temperature did not have an adverse impact on the retrieval of surface moisture. One can speculate that a large error in CBH determination has compensated for the error in surface temperature estimation. The overestimation of near-surface air temperature should have caused the retrieved surface moisture to be too large unless the lidar-estimated LCL was much lower (about 250 m) than the actual height of the LCL. However, this is unlikely since the nature of the CBH estimation from the lidar data is such that an overestimation of CBH is certainly possible, but it is unlikely that CBH could be underestimated from measurements of cloud top height unless there was an error in the cloud top height measurement itself. This possibility was checked, but no error was found. It is more likely that the relatively stable MABL has inhibited vertical mixing and thus the assumption of a well-mixed layer from the ground to the LCL is not valid in this case. In theory, if the layer is not well mixed, then surface moisture cannot be reliably obtained using our method. This result indicates otherwise but may simply be fortuitous.

The southernmost retrieval of the flight on 17 September shown in Fig. 11 (drop 13) was acquired close to the center of a subtropical high pressure center in a region of light winds and very shallow MABL depth. As is seen from the observed profiles in Fig. 11, the MABL height was 100 m or less. There was also an elevated mixed layer or residual layer above the MABL reaching to a height of about 900 m, which is most likely of continental origin. The retrieval was made using the aerosol backscatter from the ground up to about 1.0 km. The detected aerosol boundaries were, however, confined to the very shallow MABL and the top portion of the residual layer. This is why the retrieved profiles in Fig. 11 do not change with height in the region from 200 to 700 m. The observed profiles indicate a more shallow MABL than the retrieved profiles and once again demonstrates the expected difference between a point measurement (the dropsonde) and a spatial average (the retrieval).

On 15 September 1994, the P-3B flew from Ascension Island to Capetown, South Africa, on a flight path parallel to, but about 2000 km west of, the 17 September flight track. Figure 12 (drop 12) shows the observed and calculated profiles based on data taken at about 36°S. This is the southernmost dropsonde location and, like the retrieval in Fig. 10, is over relatively cool ocean water (about 15°C). The MABL is quite deep, extending to 2.3 km, and is also fairly stable. Despite the slightly stable subcloud layer, the surface moisture and temperature are retrieved to within 1 g kg^{-1} and 1°C, respectively. The slopes of the retrieved moisture and potential temperture profiles are also in good agreement with observation. The stability of the MABL is similar to that of Fig. 10 and again demonstrates that we are able to obtain accurate surface moisture retrievals even when the MABL is slightly stable. Figure 13 (drop 8) shows the retrievals from the northernmost dropsonde point on 15 September (latitude 9°S). Here, the water temperature is about 21°C, and the MABL is more well mixed than

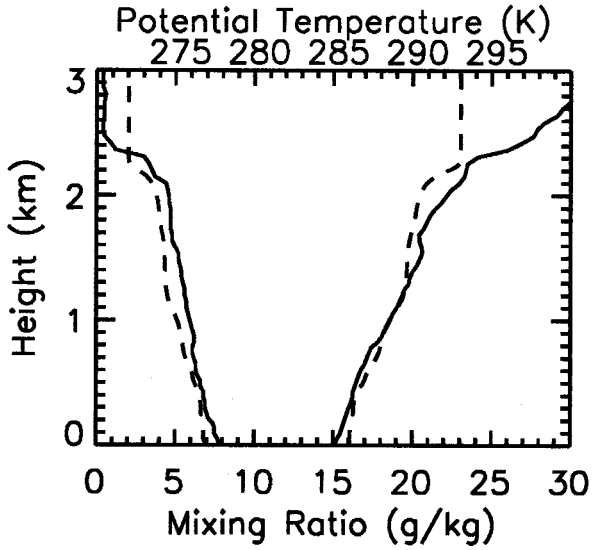

FIG. 12. Same as Fig. 8 except for drop 12, 0347 UTC 15 September 1994.

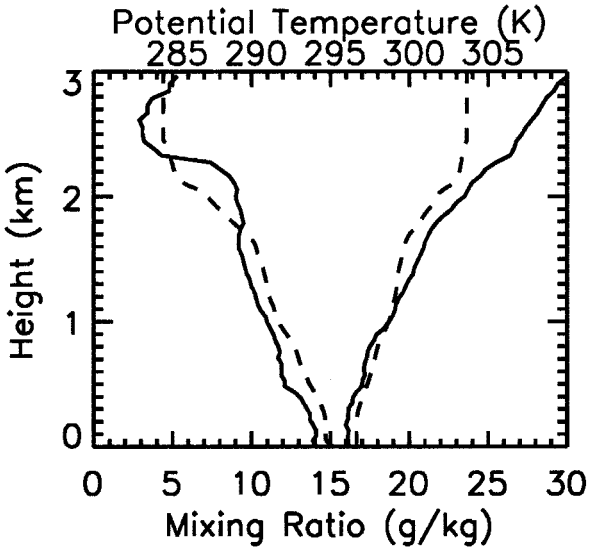

FIG. 14. Same as Fig. 8 except for drop 7, 0609 UTC 13 September 1994.

in the region of Fig. 12. The dropsonde profiles show a very well mixed subcloud layer up to about 700 m and then a slightly stable cloud layer up to the MABL top at about 1.7 km. The retrieved surface moisture is within about 1.5 g kg^{-1} of observation. The retrieved profiles show very good agreement in shape, but the retrieved moisture is about 1.0 g kg^{-1} lower than the dropsonde. Also, the height of the MABL, as indicated from the dropsonde, is about 250 m higher than the retrievals. This is again showing the magnitude of the variance of moisture and temperature within the MABL and the variance of the height of the MABL as well.

On 13 September 1994 we flew from Barbados to Ascension Island. Figure 14 (drop 7) displays the results of the southernmost retrieval for this day, taken at about 9°S, which is a few hundred kilometers off the eastern coast of Brazil. The observations show a relatively shallow well-mixed layer about 400 m deep with a slightly stable cloud layer above and continuing to the top of the MABL at around 2.2 km. The surface moisture retrieval is about 1.0 g kg^{-1} higher than the dropsonde, but the shape of the retrieved profile matches the sonde closely until near the top of the MABL. Figure 15 (drop 6) shows the data from the dropsonde launch just a few hundred kilometers northwest of the data in Fig. 14 at about 5°S. A well-mixed layer extends from the surface

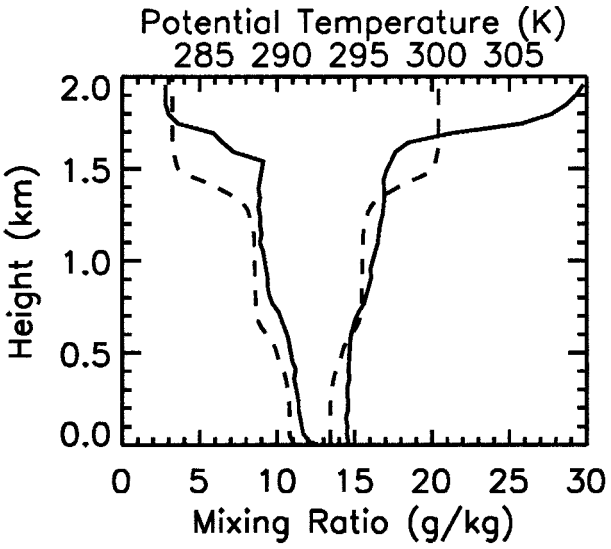

FIG. 13. Same as Fig. 8 except for drop 8, 2230 UTC 14 September 1994.

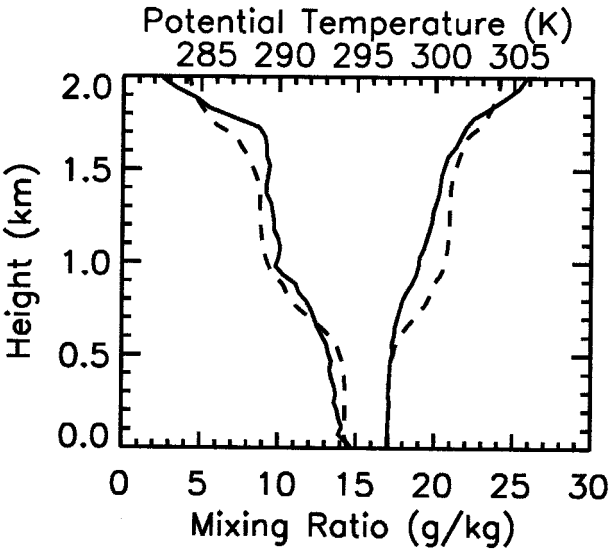

FIG. 15. Same as Fig. 8 except for drop 6, 0526 UTC 13 September 1994.

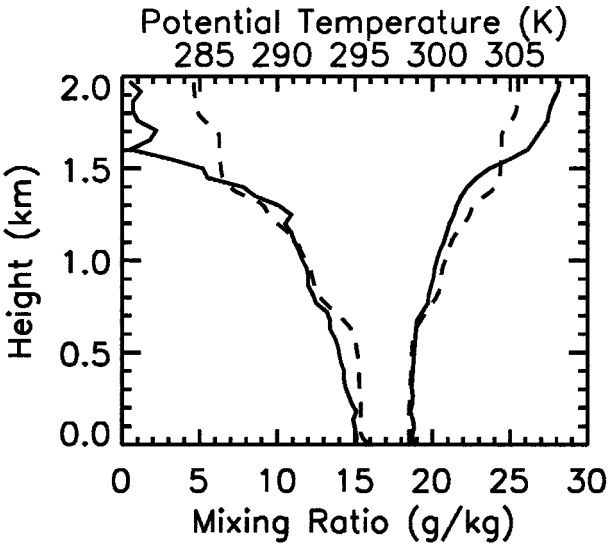

FIG. 16. Same as Fig. 8 except for drop 2, 0621 UTC 11 September 1994.

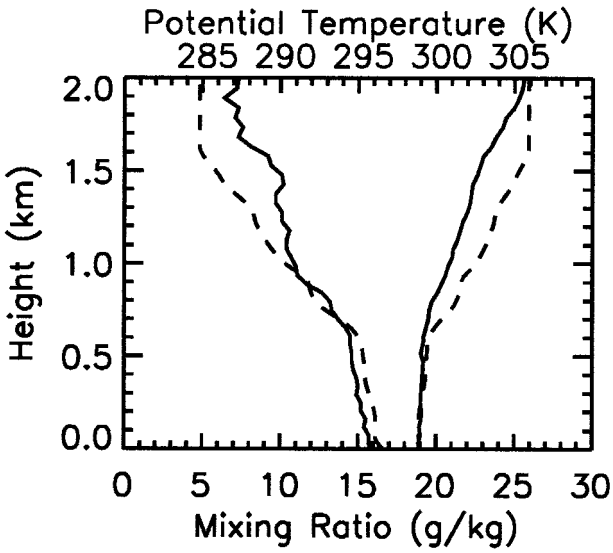

FIG. 17. Same as Fig. 8 except for drop 1, 0437 UTC 11 September 1994.

to about 700 m with a slightly stable layer from there to the MABL top at about 1.9 km. The retrievals are very good, especially within the subcloud layer. The retrieved surface moisture and average MABL moisture agree with observation to within 0.2 g kg^{-1} and 0.3 g kg^{-1}, respectively.

On 11 September 1994, the NASA P-3B began its journey around the Atlantic Ocean flying from Wallops Island, Virginia, to the island of Barbados in the Caribbean. On this flight, LASAL ran in the across-track scan mode, as discussed in section 4b. Consequently, since only the nadir shots were used from the data, the horizontal resolution is much less than the nadir-only mode. Apparently, the lower-data resolution did not affect the retrieved surface moisture or profiles, as is indicated in Fig. 16. The dropsonde, which was launched at about 19°N, shows a well-mixed layer extending to about 700 m and a slightly stable cloud layer from there to the MABL top at about 1.5 km. The SST in this region is the warmest encountered during the underflights, with values approaching 28°C. The highest mixing ratios are also found here, with values as high as 16 g kg^{-1}. The retrieved profiles closely follow the shape of the observations and the moisture profile shows the greatest discrepancy in the upper well-mixed layer at about 500 m. The final retrieval is shown in Fig. 17, which was made from data taken at about 27°N. Here, we see a well-mixed layer up to around 600 m with the familiar slightly stable cloud layer above. The top of the MABL is not well defined from the dropsonde measurements, but it appears to be around 1.7 km. The lidar data indicate a lower MABL top at about 1.5 km. The θ and q profiles are very good from the surface through the well-mixed layer but are notably different than the dropsonde above 700 m.

Table 2 summarizes the retrieval results by listing the launch or retrieval number (the date, time, and location of which is listed in Table 1), the observed and derived near-surface mixing ratio, q_0 (g kg^{-1}), the observed and retrieved averge MABL mixing ratio, $\overline{q}$ (g kg^{-1}), and the observed and retrieved average MABL potential temperature, $\overline{\theta}$ (K). The asterisk (*) identifies those retrievals that are discussed above and shown in Figs. 8–17. Also listed is the rms error for the surface moisture, average MABL moisture, and average potential temperature based on comparison with the dropsonde. The results shown in Table 2 indicate that the lidar data taken in scanning mode (drops 1, 2, 13, and 14), and hence with relatively low horizontal resolution, did not affect the near-surface moisture estimate or the bulk MABL retrieved moisture. Further, only 3 of the 16 retrievals show an error in near-surface mixing ratio of greater than 1.0 g kg^{-1}. Elimination of these three retrievals would bring the rms error of the remaining 13 down to 0.57 g kg^{-1}. There does not appear to be a correlation of retrieved mixing ratio error with MABL stability or SST. It is not known why these three retrievals show larger error than the others. It may simply be that the MABL in these areas had greater horizontal variability (of temperature and moisture) that is manifested in the comparison of the spatially averaged retrieval with the point measurement of the dropsonde.

Inspection of Figs. 9–17 indicates that the retrievals are generally better in the middle and lower part of the MABL and become less accurate toward the top third of the MABL. In this region, which is generally within the cloud layer, the retrieved q values are usually too low. Sometimes, as in Fig. 17, this is related to a poor estimate of the mixing ratio value above the MABL (q_t). More likely, the underestimation of q in the upper portion of the boundary layer is related to the presence of

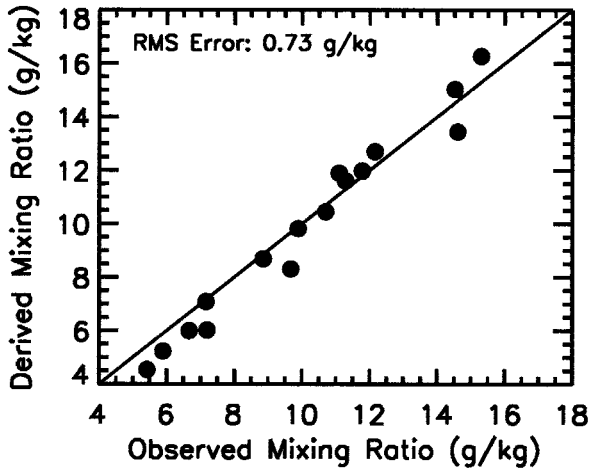

FIG. 18. A comparison of the 16 dropsonde-observed average MABL mixing ratios and the corresponding lidar–radiometer retrieved values.

clouds. Perhaps the condensation and eventual evaporation of clouds enhance the mixing process in this layer. Release of latent heat through condensation would also tend to increase turbulent mixing. Radiative effects may also play a role. The underestimation of q in the cloud layer could easily be corrected by ''weighting'' the occurrence of clouds in the cumulative probability distribution of aerosol gradients (Fig. 7). In other words, when a cloud is encountered, it would count not for one aerosol gradient, but two or three. This would have the effect of shifting the probability distribution curve upward, hence increasing the value of the retrieved q in the cloud layer. However, there appears to be no sound physical reasoning for doing so.

One interesting thing about all of the retrievals is how well the overall shape of the profiles, both mixing ratio and potential temperature, is replicated by this relatively simplistic technique. Even in cases such as Fig. 13 or 14, where the surface potential temperature estimate (which is based on the radiometric sea surface temperature) and/or the surface mixing ratio are in poor agreement with observation, the shape of the profiles is extremely good. This indicates that the basic hypothesis underlying the technique, namely, that the MABL temperature and moisture structure is determined by the frequency of convective cells rising from the surface and depositing their properties throughout the rest of the MABL, is sound.

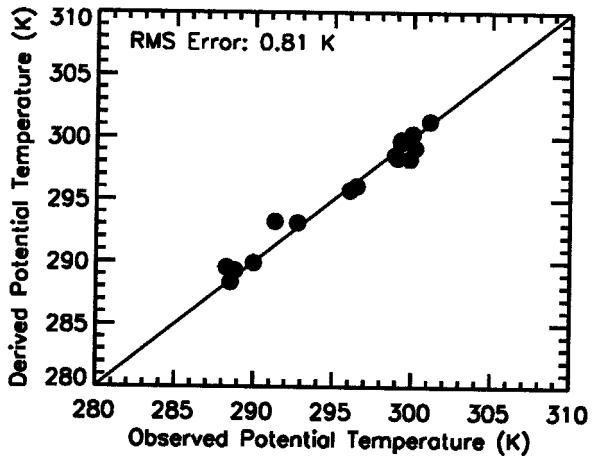

FIG. 19. A comparison of the 16 dropsonde-observed average MABL potential temperatures and the corresponding lidar–radiometer retrieved values.

The integrated water vapor amount through the depth of the MABL is very important since the MABL contains a large fraction of the total atmospheric column water vapor amount. The accuracy of retrieved water vapor profiles can be gauged by comparing the observed and retrieved average MABL water vapor (see Table 2). This is calculated by summing the profiles from the ground to the top of the MABL, as defined by the lidar [where $P(z) = 0$] and dividing by the total number of data points within that vertical range. Figure 18 shows that in terms of bulk MABL moisture content, this technique is able to provide accuracies on the order of 0.7 g kg^{-1} or about 7%. If only the lower 500 m of the MABL are considered, the accuracy of the average MABL moisture content increases to about 0.6 g kg^{-1}, which is a very respectable 5%.

The potential temperature retrievals through the depth of the MABL are also extremely good. Figure 19 shows a scatterplot of the observed average MABL potential temperature versus the lidar–radiometer-retrieved value. The rms error is 0.8°C. The average MABL potential temperature ranges between 288 and 301 K and are highly correlated with SST.

6. Summary and conclusions

A new remote sensing technique that utilizes airborne aerosol lidar backscatter data and IR radiometer data to retrieve moisture and temperature profiles through the depth of the MABL has been presented. Results suggest that the technique is applicable about 75% of the time over the tropical and subtropical Atlantic Ocean and that average MABL moisture content can be retrieved with an rms error typically on the order of 0.7 g kg^{-1}. Surface mixing ratios can be retrieved with rms errors of 0.8 g kg^{-1}. Accuracies improve to 0.6 g kg^{-1} when considering only the layer between the surface and 500 m. The retrievals show the most agreement with dropsonde measurements in the lower and middle MABL, with a larger discrepancy occurring in the higher region of the MABL or cloud layer. The magnitude of the observed rms diferences between retrieval and observation is in agreement with expected differences between a point measurement and a spatial average for a tropical or subtropical oceanic boundary layer. The profiles of potential temperature through the depth of the MABL also displayed very good agreement with ob-

servation. Implicit in the retrievals of both temperature and moisture is the assumption that the air temperature close to the surface is about 0.8°C less than the IR-derived sea surface temperature. While there were a few cases where this did not appear to be an accurate assumption (see Fig. 10 for example), it did not affect the accuracy of the retrieved surface moisture or impact the overall shape of the profiles, which closely matched observation.

The horizontal resolution of the lidar data did not seem to affect the accuracy of the near-surface moisture retrieval or the estimated profiles. This indicates that the low-resolution data (about 350 m), which were the extracted nadir shots from the scanning data, are adequate for the estimation of LCL from cloud top heights and the mapping of convective plume boundaries for the generation of moisture and temperature profiles. This makes good physical sense since the size of cumulus clouds are similar to the size of convective cells that generally scale between two to four times the depth of the MABL. Thus, the low-resolution data will provide about 10–20 samples over a typical cumulus cloud.

The applicability of this combined lidar–radiometer approach for the retrieval of MABL moisture and temperature is limited to areas of the globe where the sea–air temperature difference is within 1°–2°C. The data presented here were acquired from almost 30°N to 36°S with no major deviation from this assumption being encountered. The largest sea–air temperature difference seen was about 3.0°C over cool water, fairly close to the African continent. The data were, however, collected during the month of September in regions of normally small air temperature variation. In the winter months, cold air moving over the ocean from the continents can substantially increase the sea–air temperature difference in areas as far as 1000 km from the coast. Weller et al. (1995) report brief periods of sea–air temperature difference in the 3°–6°C range following the passage of strong cold fronts during FASINEX. These episodes did not last long, and the sea–air temperature difference quickly returned to the range of 0.5°–1.5°C.

Another consideration worth mentioning is the possible diurnal effect of solar insolation on SST in the Tropics. The skin temperature of the ocean, under light wind conditions with little vertical mixing, can easily become a degree or two warmer than the nighttime value (Hagan et al. 1997). This would tend to make the atmospheric surface layer more unstable, possibly causing the retrieved surface mixing ratios to be too high. Ideally, a similar study would be conducted both day and night to address these questions. The other limiting factor for the applicability of the technique, and one of likely greater significance, is cloud cover. Especially from space, a lidar will frequently encounter cloud cover that is optically thick enough to make MABL observations impossible. These would include areas of tropical storms, hurricanes, extratropical cyclones, and the persistent low stratus typically found off the western coast of major continents. In spite of these considerations, we believe the method could be used successfully over roughly 60% of the ocean's surface at any given time. Better coverage could be obtained in the summer hemisphere.

This technique may also work over land as well, with the surface temperature provided by observation (ECMWF initial state analysis for instance) instead of deduced from SST. In this case, however, the retrievals would be limited to the daytime since it relies on both a well-mixed PBL and the presence of cumulus clouds at the PBL top that usually dissipate shortly after sunset.

We believe that this technique has potential for remote sensing of MABL moisture and temperature from space and demonstrates the usefulness of combining passive and active remote sensing instruments. Further, the accuracy of the surface mixing ratios suggest that with the addition of a microwave sensor to infer surface wind speed, meaningful surface latent heat fluxes over the ocean could also be obtained using the bulk aerodynamic method.

Acknowledgments. The authors would like to thank the following people who have helped to make this paper a reality. Dr. Pat McCormick, principal investigator of the LITE project, for providing aircraft flight time and data analysis funding: Dean Lauritsen and Larry Murphy from the National Center for Atmospheric Research (NCAR), who provided the dropsonde measurements; Keith Evans, who helped with lidar and NOAA sea surface temperature data analysis; Dave Carter, who was the lead engineer and project manager for the LASAL system; James Marsh, also an engineer, provided expertise ranging from the installation and maintenance of the LASAL system to the software that ran LASAL's scanning motor; Doug Young, Dave Pierce. Evan Webb, and Roger Navaro of Wallops Flight Facility for their timely mission planning and support; and the crew of the NASA P-3B for their help in the installation of the science instruments and their diligent efforts in maintaining and operating the aircraft.

REFERENCES

Boers, R., E. Eloranta, and R. Coulter, 1984: Lidar observations of mixed layer dynamics: Tests of parameterized entrainment models of mixed layer growth rate. *J. Climate Appl. Meteor.*, **23,** 247–266.

Carswell, J., S. Carson, R. McIntosh, F. Li, G. Neumann, D. McGlaughlin, J. Wilkerson, P. Black, and S. Nghiem, 1994: Airborne scatterometers: Investigating ocean backscatter under low- and high-wind conditions. *Proc. IEEE,* **82,** 1835–1860.

Chang, H. D., P. H. Hwang, T. T. Wilheit, A. T. C. Chang, D. H. Staelin, and P. W. Rosenkranz, 1984: Monthly distributions of precipitable water from the *Nimbus-7* SMMR data. *J. Geophys. Res.,* **89,** 5238–5334.

Chou, S.-H., and D. Atlas, 1982: Satellite estimates of ocean–air heat fluxes during cold air outbreaks. *Mon. Wea. Rev.,* **110,** 1434–1450.

——, R. Atlas, C.-L. Shie, and J. Ardizzone, 1995: Estimates of

surface humidity and latent heat fluxes over oceans from SSM/I data. *Mon. Wea. Rev.,* **123,** 2405–2425.

Dalu, G., 1986: Satellite remote sensing of atmospheric water vapor. *Int. J. Remote Sens.,* **7,** 1089–1097.

Ferrare, R. A., J. Schols, and E. Eloranta, 1991: Lidar observations of banded convection during BLX83. *J. Appl. Meteor.,* **30,** 312–326.

Grant, D. R., 1965: Some aspects of convection as measured by aircraft. *Quart. J. Roy. Meteor. Soc.,* **91,** 268–281.

Hagan, D., 1988: The profile of upwelling 11-micron radiance through the atmospheric boundary layer overlying the ocean. *J. Geophys. Res.,* **93,** 5294–5302.

——, D. Rogers, C. Friehe, R. Weller, and E. Walsh, 1997: Aircraft observations of sea surface temperature variability in the tropical pacific. *J. Geophys. Res.,* **102,** 15 733–15 747.

Hartman, D., 1994: The scientific importance of GLAS atmospheric measurements. *Earth Observ.,* **6,** 5–9.

Higdon, N. S., and Coauthors, 1994: Airborne differential absorption lidar system for measurements of atmospheric water vapor and aerosols. *Appl. Opt.,* **33,** 6422–6438.

Hock, T., and H. Cole, 1991: A new aircraft universal lightweight digital dropsonde. Preprints, *Seventh Symp. on Meteorological Observations and Instrumentation,* New Orleans, LA, Amer. Meteor. Soc., 291–296.

Kaimal, J. C., N. Abshire, R. Chadwick, M. Decker, W. Hooke, R. Kropfli, W. Neff, F. Pasqualucci, and P. Hildebrand, 1982: Estimating the depth of the daytime convective boundary layer. *J. Appl. Meteor.,* **21,** 1123–1129.

Konrad, T. G., and F. Robison, 1973: Development and characteristics of free convection in the clear air as seen by radar and aircraft *J. Appl. Meteor.,* **12,** 1284–1294.

Lenschow, D. H., 1970: Airplane measurements of planetary boundary layer structure. *J. Appl. Meteor.,* **9,** 874–884.

Liu, W. T., 1986: Statistical relation between monthly mean precipitable water and surface-level humidity over global oceans. *Mon. Wea. Rev.,* **114,** 1591–1602.

——, 1988: Moisture and latent heat flux variabilities in the tropical Pacific derived from satellite data. *J. Geophys. Res.,* **93,** 6749–6760.

——, and P. P. Niiler, 1984: Determination of monthly mean humidity in the atmospheric surface layer over oceans from satellite data. *J. Phys. Oceanogr.,* **14,** 1451–1457.

McCormick, M., and Coauthors, 1993: Science investigations planned for the Lidar In-Space Technology Experiment (LITE). *Bull. Amer. Meteor. Soc.,* **74,** 205–213.

McCormick, P., 1995: Spaceborne lidars. *Rev. Laser Eng.,* **23,** 89–93.

Melfi, S. H., J. Spinhirne, S.-H. Chou, and S. Palm, 1985: Lidar observations of vertically organized convection in the planetary boundary layer over the ocean. *J. Climate Appl. Meteor.,* **24,** 806–824.

Palm, S. P., S. H. Melfi, and D. L. Carter, 1994: New airborne scanning lidar system: Applications for atmospheric remote sensing. *Appl. Opt.,* **33,** 5674–5681.

Prabhakara, C., and G. Dalu, 1979: Remote sensing of seasonal distribution of precipitable water vapor over the oceans and the inference of boundary layer structure. *Mon. Wea. Rev.,* **107,** 1388–1401.

——, ——, and V. G. Kunde, 1974: Estimating of sea surface temperature from remote sensing in the 11 to 13 μm window region. *J. Geophys. Res.,* **79,** 5039–5044.

Sasano, Y., H. Shimizu, and N. Takeuchi, 1982: Convective cell structures revealed by a Mie laser radar observation and image data processing. *Appl. Opt.,* **21,** 3166–3169.

Schluessel, P., 1989: Satellite-derived low-level atmospheric water vapour content from synergy of AVHRR and HIRS. *Int. J. Remote Sens.,* **10,** 705–721.

——, and W. Emery, 1990: Atmospheric water vapour over oceans from SSM/I measurements. *Int. J. Remote Sens.,* **11,** 753–766.

Schulz, J., P. Schluessel, and H. Grassl, 1993: Water vapour in the atmospheric boundary layer over oceans from SSM/I measurements. *Int. J. Remote Sens.,* **15,** 2773–2789.

Skony, S. M., and J. D. Kahl, 1994: Differences between radiosonde and dropsonde temperature profiles over the Arctic Ocean. *J. Atmos. Oceanic Technol.,* **11,** 1400–1408.

Stull, R., and E. Eloranta, 1983: A case study of the accuracy of routine, fair-weather cloud-base reports. *Natl. Wea. Dig.,* **10,** 19–24.

Vandemark, D., F. Jackson, E. Walsh, and B. Chapron, 1994: Airborne radar measurements of ocean wave spectra and wind speed during the Grand Banks *ERS-1* SAR wave experiment. *Atmos.–Ocean,* **32,** 143–178.

Wagner, D., E. Ruprecht, and C. Simmer, 1990: A combination of microwave observations from satellites and an EOF analysis to retrieve vertical humidity profiles over the ocean. *J. Appl. Meteor.,* **29,** 1142–1157.

Warner, J., and J. W. Telford, 1967: Convection below cloud base. *J. Atmos. Sci.,* **24,** 374–382.

Webster, P. J., C. A. Clayson, and J. A. Curry, 1996: Clouds, radiation, and the diurnal cycle of sea surface temperature in the tropical western Pacific. *J. Climate,* **9,** 1712–1730.

Weller, R. A., D. L. Rudnick, and N. J. Brink, 1995: Meteorological variability and air–sea fluxes at a closely spaced array of surface moorings. *J. Geophys. Res.,* **100,** 4867–4883.

Whiteman, D. N., S. H. Melfi, and R. A. Ferrare, 1992: Raman lidar system for the measurement of water vapor and aerosols in the earth's atmosphere. *Appl. Opt.,* **31,** 3068–3082.